Light-Emitting Porous Silicon: Materials Science, Properties, and Device Applications

Silicon-based, light-emitting devices (LED's) should find numerous uses in optoelectronics. For example, the integration of silicon LED's with silicon microelectronics could lead to reliable and inexpensive optical displays and optical interconnects. Until recently, however, it had not been possible to obtain efficient room-temperature luminescence from silicon. The demonstration in 1990 that a form of silicon called "porous" can emit bright photoluminescence in the red region of the spectrum triggered worldwide research efforts aimed at establishing the mechanisms for the unexpected luminescence and at fabricating efficient and durable LED's. In less than five years, significant progress has been achieved on both fronts. LED's emitting throughout the visible spectrum have been demonstrated, and the best measured external electroluminescence efficiency has risen from $10^{-5}\%$ to better than 0.01% at room temperature. The photoluminescence efficiency of the best samples is near 10% at room temperature, and light-emitting porous silicon (LEPSi) that luminesces from the blue part of the spectrum to the infrared beyond 1.5 μm has been produced. In this article, we first review why silicon is a poor light emitter and then define porous silicon and its main properties. We then focus on the properties of the three luminescence bands ("red," "blue," and "infrared") and present the results of femtosecond time-resolved optical measurements. Next, we report progress toward the fabrication of LED's and discuss some specific device structures. Finally, we outline what is necessary for commercial LEPSi LED's to become a reality and report on experimental results that suggest the possible integration of LEPSi with standard microelectronic devices.

Porous Silicon

1. Silicon Light Emission

Radiative recombination of an electron with a hole across the bandgap of semiconductors produces luminescence. The emitted photons have an energy equal to the bandgap energy (e.g., 1.4 to 1.5 eV in GaAs) and negligible momentum. Thus, the electron and the hole must be located at the same point in the Brillouin zone, which is the case in direct-gap semiconductors such as GaAs. Under these conditions, the radiative recombination rate is large, which means that the radiative lifetime is short (typically of the order of a few nanoseconds). To obtain a large luminescence efficiency, the nonradiative recombination rate must be lower than the radiative recombination rate. The efficiency is defined as

$$\eta = \tau_{\text{nonrad}} / \left(\tau_{\text{nonrad}} + \tau_{\text{rad}}\right), \tag{1}$$

where η is the quantum efficiency, τ_{rad} is the radiative lifetime, and τ_{nonrad} is the nonradiative lifetime. Nonradiative recombination occurs both at the surface and in the bulk. To minimize it, the surface should be well passivated leading to a low surface recombination velocity S, and the bulk must be free of defects that act as radiation killers. The efficiency of good-quality, direct-gap III–V semiconductors exceeds 1% at room temperature and 10% at cryogenic temperature.

Because silicon is an indirect-gap semiconductor, electrons and holes are found at different locations in the Brillouin zone and recombination by emission of a photon alone is not possible. Photon emission is possible only if another particle capable of carrying a large momentum, such as a phonon, is involved. In this case, both energy and momentum can be conserved in the radiative transition. The participation of a third particle in addition to the electron and the hole makes the rate of the process substantially lower and the radiative lifetime typically in the millisecond regime. Thus, the efficiency drops by several orders of magnitude, even in the case of high-purity materials and good surface passivation. At room temperature, the typical efficiency of crystalline silicon is of the order of $10^{-5}\%$, which makes it unsuitable for LED's.[1] Several attempts have been made to improve the luminescence efficiency of silicon and silicon-based alloys, including the use of silicon-germanium alloys and superlattices,[2] isoelectronic impurities[3] in a manner similar to nitrogen in GaP, and erbium doping.[4] The strategy in these attempts can be divided into two classes: increasing the radiative rate or decreasing the nonradiative rate. The former can be achieved by "bandgap engineering" or "defect engineering," which essentially consists of "convincing" the electron and the hole that they do not

require a phonon to recombine radiatively. This process can be accomplished through zone folding in thin superlattices or with isoelectronic impurities whose energy level extends throughout the Brillouin zone. The latter consists of confining the electron and the hole to a small volume where the probability of finding a nonradiative center is equal to zero. This can be accomplished in the Ge-rich regions of SiGe and is realized to some extent with isoelectronic impurities. Such approaches have led to very good photoluminescence efficiencies (up to 10% in some cases) and good electroluminescence efficiency in some structures (approaching 1%), but only at cryogenic temperatures. At room temperature, these numbers drop to the range of 10^{-4}% to 10^{-5}%, and it is not clear how they can be increased to the 0.1% to 1% level.

2. Porous Silicon

Porous silicon is a material that has been known for nearly 40 years.[5] It has found limited use in microelectronics,[6] especially in the silicon-on-insulator (SOI) technology, as porous silicon becomes a good insulator after oxidation. In the 1980's, several studies of the optical properties of porous silicon were published, and photoluminescence in the deep red/near infrared was detected at cryogenic temperatures.[7] In 1990, Canham[8] reported that when porous silicon is further etched in concentrated aqueous HF for 6 h after preparation, it emits bright red light when illuminated with blue or UV light. Longer etching in HF was demonstrated to lead to brighter photoluminescence at shorter wavelengths, which was ascribed to quantum confinement. Longer etching increases the porosity, which produces, on the average, smaller nanocrystalline columnar structures. When the dimension of the columns decreases below 5 nm, the bandgap widens by quantum confinement in the conduction and valence bands and thus smaller columns produce larger bandgaps. In Canham's original model, the luminescence was attributed to band-to-band recombination across the bandgap. He also suggested that porous silicon might have a direct bandgap, which would explain the increase in efficiency by several orders of magnitude. Interestingly, at the same time as Canham was publishing his seminal paper, Lehmann and Gosele[9] independently showed that the bandgap of porous silicon is larger than that of crystalline silicon and attributed this increase to quantum confinement as well.

Lehmann and Gosele's proposal allowed them to provide a new and elegant explanation for the mechanism of pore formation. Injection of holes from the substrate to the surface is required for etching in HF. In their model, the thinning of the silicon columns formed when the pores are created continues until quantum confinement produces a barrier against hole transport into the columns. Although there are attractive competing models,[10] which for example rely on electrostatic effects near the pore's tip, this model has received partial experimental confirmation.[11] It must be noted that neither Canham's model for the luminescence nor Lehmann and Gosele's model for pore formation is universally accepted, and other models have been proposed.[12–16] Note also that the nanostructure of porous silicon is quite complicated. Even though columnar crystalline structures are present in some samples, the shape, thickness, and orientation of these columns or wires are not uniform. In other samples, no wires are detected, and the crystalline objects appear to be more or less spherical ("dots"). In all cases, however, light emission appears to be well correlated with the presence of crystalline structures smaller than 5 nm.[17]

Figure 62.36 shows the schematic arrangement for a typical electrochemical cell used to produce porous silicon. The arrangement is very simple and inexpensive. The wafer (anode) and the metal cathode are immersed in an aqueous solution containing HF. Typically, the HF concentration is kept around 25% by weight, and ethanol or methanol is added to improve the penetration of the solution into the pores and to minimize hydrogen bubble formation. Maintaining a constant current density of 1 to 100 mA/cm^2 for several minutes results in the formation of a porous silicon film with a thickness ranging from ~1 μm to tens of microns. Both the thickness and the photoluminescence spectrum of the porous layer depend

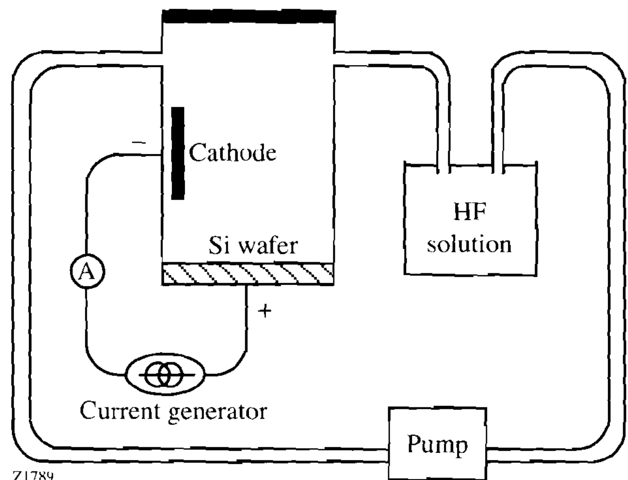

Figure 62.36
Schematic of the electrochemical cell used for the production of porous silicon. The HF solution circulates in Teflon™ tubing and through a Teflon™ pump.

strongly on many parameters, such as doping level and sign, current density, solution concentration and pH, and duration of the anodization. However, it should be stressed that light-emitting porous silicon can be produced over a wide range of most of these parameters. For example, holes, which play a critical role in the formation of porous silicon, cannot be injected from the bulk to the surface of an n-type wafer. This shortcoming can be eliminated by illuminating the wafer during anodization, as holes are photogenerated near the surface. Even if the porous layer is not of the luminescent type, further etching in HF in the open circuit configuration or by anodic oxidation in water can produce bright luminescence.

Figure 62.37 shows a LEPSi luminescence spectrum and its time evolution after pulsed excitation at 3.5 eV. The peak photoluminescence wavelength is typical, but it can easily be tuned between 850 nm and 550 nm, as discussed later. The full-width at half-maximum (FWHM) of the spectrum is between 150 meV and 500 meV. The most widely accepted explanation for this very large width is that the spectrum is "inhomogeneous," i.e., corresponds to bandgap or near-bandgap emission coming from nanocrystallites with a distribution of sizes. The decay of the photoluminescence following excitation takes place on a microsecond time scale at room temperature and increases to the millisecond regime at cryogenic temperatures.[18] Furthermore, the short-wavelength components usually decay faster than the long-wavelength components, a fact that also supports the hypothesis that a distribution of crystallite sizes produces the wide spectrum. This spectral diffusion with time varies from sample to sample. The decay of the full band or that of any individual wavelength component does not follow a simple law and can be fitted very well using a stretched exponential function.[19] Stretched exponentials may result from the random walk of carriers on a finite distribution of discrete sites in real space, as is known to occur in amorphous silicon. Regardless of the details of the physical mechanisms, there are well-known procedures to define the average or most probable lifetime; this lifetime value is usually quoted in the literature. After removing a possible fast decay component in the nanosecond time domain (to be discussed later), the lifetime of the red luminescence is in the microsecond time domain.

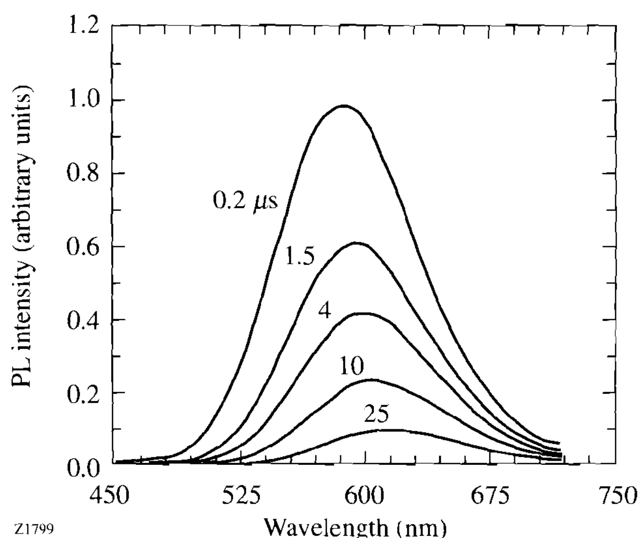

Figure 62.37
Time-resolved photoluminescence spectra measured at different times following excitation with a picosecond laser pulse at 3.5 eV. The overall decay at room temperature is in the microsecond time domain, but the decay is not exponential and is faster at shorter wavelengths.

The Three Luminescence Bands

1. The Red Band

As mentioned earlier, the "red" luminescence band actually extends from the near infrared to the orange/green regions. Tuning can be achieved by changing any one of many parameters.[20] Here, we focus on results obtained by changing the anodization time under light assistance and by annealing in air. The LEPSi samples were prepared from p-type Si substrates in the dark (DA) or from p- and n-type Si substrates with light assistance (LA). The substrates were (100) oriented with a resistivity in the 1- to 10-Ω-cm range. Anodization with LA was performed using a 300-W, white-light halogen lamp.

The photoluminescence (PL) spectra from DA and LA samples are rather different.[21] The DA LEPSi has a broad peak centered near 740 nm, which is typical of samples prepared in the dark. In contrast, the PL spectra of the LA samples can be easily tuned from the infrared to the yellow/orange by increasing the anodization time. For a given solution and a constant current density, a longer anodization time produces a thicker LEPSi layer and shifts the PL peak toward shorter wavelengths. Figure 62.38 shows the relation between PL intensity, PL peak wavelength, and anodization time for n-type Si wafers prepared in an aqueous solution (no alcohol) with LA using a current density j of 10 mA/cm^2.[22] Under these conditions, the maximum PL intensity corresponds to a peak wavelength near 700 nm. A proper choice of solutions and current density allows us to obtain homogeneous LEPSi samples that have good PL efficiency. Using blue excitation, the highest quantum efficiency we have measured on a red LEPSi sample at room temperature is approximately 5%. After optimization of the growth conditions, the PL of LEPSi samples is comparable to that emitted at room temperature by direct-gap III–V semiconductor compounds.

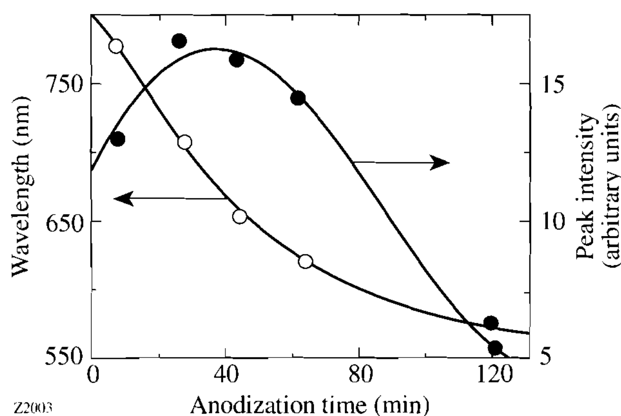

Figure 62.38
Photoluminescence intensity and peak wavelength as a function of the anodization time. The current density is 10 mA/cm^2, the substrate is a 10-Ω-cm *n*-type Si wafer, and light assistance is employed.

The PL peak wavelength has also been tuned by thermal annealing in a tube furnace in ambient air for 5 min at various temperatures.[23] In this case, the LEPSi layers were formed by anodization in the dark of 10-Ω-cm *p*-type Si wafers in a 1:1:2 solution of HF, H_2O, and methanol. Figure 62.39 summarizes results obtained with a variety of samples, either freshly prepared, annealed in air, or oxidized in HNO_3. The PL peak wavelength shifts to shorter values as the ratio of Si-O bonds to Si-H bonds increases. The ratio of the concentration of Si-H and Si-O bonds present on the surface of the nanocrystallites as shown in Fig. 62.39 is not the absolute ratio, since the cross section for infrared absorption of Si-O bonds is stronger than that for the Si-H bonds. Thus, the horizontal scale in Fig. 62.39 is a relative scale only. These results demonstrate a clear correlation between surface chemistry and PL peak wavelength. Freshly anodized samples that contain a very small but detectable amount of Si-O bonds and chemically oxidized samples that have almost no remaining Si-H bonds fit nicely at the two extremes of the data. Furthermore, annealing of freshly prepared samples at moderate temperature leads to data points that coincide with the data points obtained with aged samples.

The results of Fig. 62.39 are more easily understood if we assume that the PL is related to recombination involving surface states[24] rather than if it is strictly due to confinement[8] since the low-temperature treatments reported here have no effect on the particle size. For a particular surface coverage of the nanocrystallites present in LEPSi, we expect to find a specific set of surface states. When the coverage is changed, the nature and the energetic position of the surface states within the bandgap should change; thus, the PL spectrum is expected to change as well. It may be reasonable to model the wide PL spectrum as due to several bands associated with recombination involving different surface species.

It is worth noting that the origin of the "red" luminescence remains highly controversial. Many models have been proposed, ranging from those involving specific defects and molecular compounds to those involving quantum confinement.[12–16,25] Of all these models, two have received strong experimental support. The "pure" quantum confinement originally proposed by Canham,[8] which is consistent with many observations, has recently received support from resonant photoluminescence experiments.[26,27] In these experiments the low-temperature luminescence was not excited by a short-wavelength laser but by a laser tuned inside the broad PL spectrum to provide size-selective excitation. Under these conditions, the PL spectrum shows discrete steps that coincide with the zone-edge phonons of crystalline silicon that are known to be involved in the bandgap absorption and emission in crystalline silicon. These results not only indicate that silicon is the absorbing and luminescing species in LEPSi but also strongly suggest that luminescence occurs at the silicon crystallite bandgap. Other experiments, however, suggest that the luminescence occurs well below the bandgap and is affected by more than quantum confinement. Some examples include the results shown in Fig. 62.39 and the difference between the measured PL peaks and the measured or calculated bandgap,[28,29] which can be as large as ~1 eV.

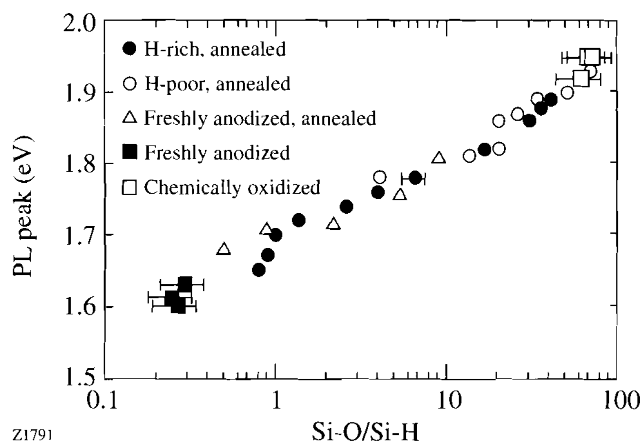

Figure 62.39
Relationship between the peak of the photoluminescence spectrum and the surface coverage, as measured by the ratio of Si-O bonds over Si-H bonds obtained by infrared absorption measurements. This ratio does not take into account the difference in the infrared absorption cross sections between Si-H and Si-O bonds.

Since the PL intensity and spectrum depend strongly on the surface coverage, one can expect some problems with long-term stability of the PL. For hydrogen-covered surfaces, the surface can become depassivated by hydrogen loss through heating[30] or exposure to short-wavelength light.[31] A solution to this problem is passivation with silicon dioxide instead of hydrogen. Such samples are much more resilient[21] but they also tend to luminesce in the blue.

2. The Blue Band

Recent literature contains several reports of strong blue PL in LEPSi after rapid thermal oxidation (RTO) at high temperature ($T_{ox} \geq 1000°C$),[32,33] as well as several reports of weaker blue PL in various samples. We conducted a systematic investigation of the properties of blue samples and have evaluated methods for obtaining them. The LEPSi layers were formed by anodization of 5-Ω-cm *p*-type silicon wafers in a 1:1:2 solution of HF, H_2O, and methanol. To change the sample's properties we varied the current density from 1 mA/cm^2 to 30 mA/cm^2. Anodization was performed either in the dark or with light assistance. Oxidation of the LEPSi layers was achieved in a tube furnace with a dry oxygen atmosphere. Samples of LEPSi first anodized in the dark at a current density $j = 10$ mA/cm^2 and then oxidized for 2 min at 1100°C in dry oxygen[34] display the reported blue PL band (Fig. 62.40). Infrared absorption measurements show a strong line at 1080 cm^{-1} related to the asymmetric stretching vibrational mode of the Si-O-Si oxygen bridge (Fig. 62.40, inset). Other LEPSi samples anodized at a smaller current density (1 mA/cm^2) with light assistance and subjected to no further treatments have only one strong peak at 1070 cm^{-1} in the infrared spectrum, which corresponds to Si-O-Si bridges in a configuration close to stoichiometry. Thus, the infrared spectra show no significant difference in the chemical composition between these two types of samples. Although we refer to these samples as "fully oxidized" in the following discussion since no Si-H bonds remain, this does not imply that there are no silicon nanocrystallites left in these samples.

The time-resolved PL spectra of both samples show a broad PL band (FWHM > 0.5 eV) with a peak near 2.6 eV that decays on a nanosecond time scale. The PL spectra have not been corrected for the spectral sensitivity of our detection system and are likely to extend to shorter wavelengths. The decay is nonexponential as for the red band, but in contrast to the red band, no significant wavelength dependence of the blue PL decay has been observed when the detection wavelength was changed from 440 nm to 650 nm, unlike what is seen in the red PL. The decay dynamics did not change appreciably when the measurements were performed at cryogenic temperatures. The observed nonexponential decay may indicate a distribution of carrier lifetimes, with the most probable lifetime being close to 1 ns. The estimated quantum efficiency of the blue PL is greater than 0.1%, roughly one order of magnitude below the efficiency of a good red sample.

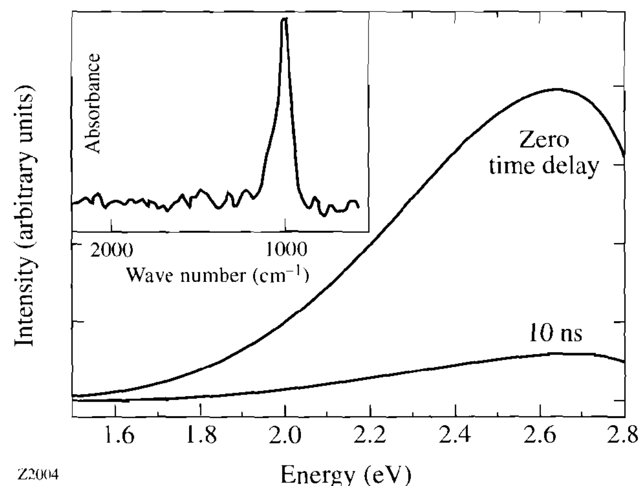

Figure 62.40
Time-resolved photoluminescence spectra of oxidized LEPSi after excitation with a picosecond laser pulse at 3.5 eV. The infrared absorption spectrum of the same sample shown in the inset indicates that the sample contains no Si-H bonds and only Si-O bonds.

The blue PL is also observed in samples that are oxidized chemically by immersion in 10% HNO_3 for 2 min or in freshly anodized samples after handling in air.[34] Measurements of the blue PL dynamics in the chemically oxidized sample also show a nonexponential decay with a characteristic time close to those of the fully oxidized samples. The time-resolved PL spectra of the freshly anodized samples measured right after excitation again show a weak but clearly observable blue PL band whose spectrum is similar to that of the "fully oxidized" samples. The presence of a very small amount of Si-O bonds is apparent in the infrared spectra of freshly anodized samples. Due to the low intensity of this blue band we were not able to analyze the decay in detail, but the characteristic decay time is much less than 15 ns.

Our results suggest two possibilities for the origin of the blue PL. Silicon dioxide is known to luminesce efficiently in the visible under appropriate conditions,[35] and it has been shown that blue PL with a nanosecond decay time can be excited by 4-eV photons in high-purity, wet synthetic silica.[36] Thus, the blue PL in oxidized LEPSi could originate not from

the silicon crystallites themselves, but from the oxide surrounding them. The second possibility is that special Si-O configurations produce the luminescence. These special configurations could be present at the Si nanocrystal/silicon dioxide interface, or in Si-rich regions produced in the oxide after nearly complete oxidation of the crystallites. It appears that we can exclude the hypothesis that the blue PL would originate from the interior of sub-3-nm Si crystallites. If this were the case, subjecting the oxidized crystallites to chemical agents should not affect the luminescence. We have exposed blue-emitting oxidized porous silicon to liquid methanol and observed a quenching of the blue PL.[37] This quenching is consistent with luminescent centers near the oxide surface. Specific chemical configurations such as silanol[38] have been proposed, but there remains considerable uncertainty as to the exact origin of the blue PL.[39] Note finally that the stability of the blue samples in air is much improved compared to that of the red samples.[21] This improvement can be traced to the presence of silicon dioxide, which is much less fragile than the Si-H bonds that passivate the surface of freshly prepared LEPSi.

3. The Infrared Band

Very few reports of infrared PL have appeared in the literature.[8,24,40–42] Some of these measurements were interpreted as bandgap or near-bandgap PL from crystalline silicon. Another explanation has been proposed for this IR PL, in which emission is associated with mid-gap dangling bonds on the surface of the nanocrystallites.[24] We have performed a careful measurement of the IR PL in several LEPSi samples.[41] In our experiments, the samples were placed in an ultrahigh vacuum (UHV) chamber where they were annealed *in situ*. The 422-nm line of a HeCd laser excites the PL, which in turn is detected by a Ge detector with a cutoff of ~0.7 eV. In the results reported below, the PL spectrum was recorded at room temperature, following vacuum annealing at temperatures as high as ~500°C for 5 min.

Figure 62.41 shows the room-temperature PL spectra for one sample before annealing and after annealing at two temperatures. The broad IR PL peak of the as-prepared sample is small but measurable at room temperature. As the annealing temperature is increased, its relative intensity increases until it dominates the spectrum. The IR PL appears to be most intense after annealing at a temperature where the red PL disappears, i.e., when most of the hydrogen that passivates the LEPSi surface has been desorbed, since heat treatment at such a temperature produces many dangling bonds. It is thus tempting to interpret the IR PL as due to recombination involving carriers in mid-gap dangling bonds. We also prepared samples in which the IR PL peak energy was ~0.7 eV. After annealing around 350°C, the integrated PL intensity measured at room temperature was comparable to the integrated intensity of the initial red PL peak. Preliminary results obtained with a luminescence detection system that is sensitive to wavelengths up to 5 μm indicate that these samples luminesce well past 2 μm. The conditions required for obtaining such samples are as of yet not well understood.

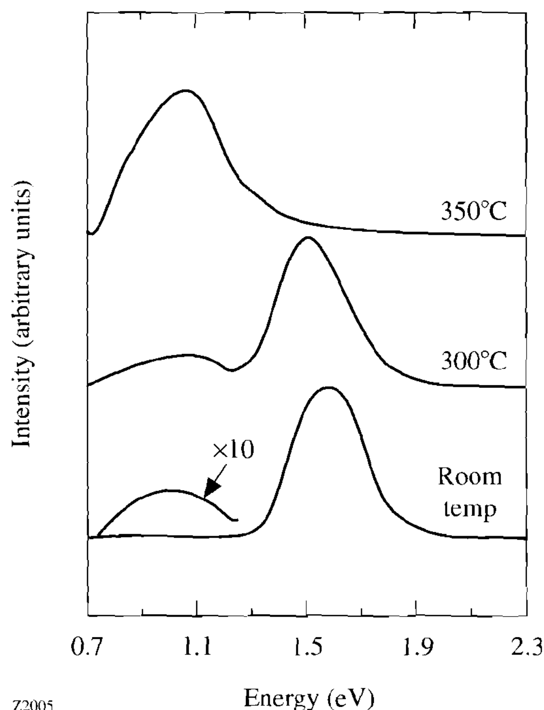

Figure 62.41
Normalized room-temperature PL spectra for LEPSi held in ultrahigh vacuum, before and after annealing for 5 min at two temperatures.

Time-resolved PL measurements[42,43] indicate a decay in the range from tens of nanoseconds to ~10 μs at 77 K, which is faster than the red PL decay in the same range of temperature. This decay may be consistent with calculations of the radiative recombination in the infrared due to dangling bonds present at nanocrystallite surfaces.[44] Finally, the long-term stability of the infrared band has not been established. If it is related to the presence of dangling bonds, it is reasonable to expect poor stability since the concentration and nature of dangling bonds on the surface can be modified by many factors. Our preliminary results so far support this hypothesis.

Femtosecond Photoinduced Absorption

1. Experimental Techniques and Sample Preparation

The femtosecond time-resolved experiments have been

performed with the standard pump/probe arrangement. The pump beam excites electrons and holes across the bandgap, while the probe beam monitors the changes in transmission (and reflection) induced in the sample by photoinjection of carriers by the pump beam. The pump and probe beams are synchronized since they are produced by the same laser pulse. Thus, the time evolution of the changes in transmission (and reflection) is monitored by increasing the beam path of the probe, which produces a time delay between the pump and probe beams. These experiments, which we routinely perform in semiconductors,[45–47] have a time resolution limited by the pulse duration (in the present case, 100 fs). Once the results have been recorded, the changes in optical properties are related to the dynamics of the photoinjected carriers, which may include thermalization, cooling, trapping, and recombination. In cases where nonradiative recombination occurs rapidly across the bandgap,[47,48] it is also possible to record the dynamics of the temperature increase of the sample due to the production of a large number of phonons.

Femtosecond photoinduced measurements were performed using two different laser systems. In the first type of experiments,[49] the laser source was a colliding-pulse, mode-locked dye laser, amplified at 8.5 kHz using a copper vapor laser. The pulses are <100 fs long at 620 nm (2 eV). A portion of these pulses is used to generate a white light continuum from which 100-fs-long pulses tunable from the green to ~900 nm were selected. In the second type of experiments,[50] the laser source was a titanium sapphire laser producing 90-fs-long pulses tunable between 800 and 900 nm (1.55 to 1.38 eV) with a repetition rate of 85 MHz. Pulses at half the wavelength (twice the photon energy) were obtained by frequency doubling in a BBO nonlinear crystal.

To perform the transmission measurements, the samples must first be removed from their silicon substrates, as the substrates would absorb all the light at wavelengths shorter than 1 μm. In the present work, we used both oxidized mesoporous films[49] and very-high-quality films deposited on sapphire.[50,51] These latter films were produced using a current density of 14 mA/cm^2 passing through a circular area of 1.76 cm^2 from 25 s to 30 min depending on the desired thickness. The anodization occurred in the dark and the (100) polished c-Si wafers were either moderately or highly doped. To remove the porous silicon film from the substrate, electropolishing was employed in which the silicon atoms were removed layer by layer and the porous silicon film was separated from the wafer (lifted off). The process was converted from porous silicon formation to electropolishing by diluting the HF while increasing the current density to approximately 100 mA/cm^2. The freestanding LEPSi films were kept wet in ethanol to protect them from breaking during drying, and layers thinner than ~5 μm were deposited wet on sapphire windows and allowed to dry in air. Afterward, the LEPSi films remained attached to the windows by van der Waals or electrostatic forces, similar to a technique used to mount ultrathin III–V semiconductor films.[45] We chose sapphire windows because of their optical flatness, high heat conductivity, and high transparency from the IR to the UV. Figure 62.42 summarizes some of the properties of a typical high-quality ultrathin LEPSi film.

2. Experimental Results

Figure 62.43 shows results obtained with the pump at 2 eV (which is well above the PL peak of 1.65 eV) and various probes at photon energies ranging from above to below the PL peak energy.[49] Qualitatively similar results have been obtained on all films, irrespective of whether they were pumped at 2 or 3 eV, in the entire probe wavelength range. These traces have several interesting features:

- At all probe wavelengths, the absorption increases instantly, then recovers in part very promptly to a photoinduced absorption "plateau."
- When the induced absorption is measured on a much longer time scale, this "plateau" corresponds in fact to a slow recovery of the photoinduced absorption.
- The recovery is nonexponential and depends on the photoinjected carrier density: at low injected carrier density, the prompt recovery is extremely fast and the slower recovery takes tens of picoseconds, whereas at high injected carrier density, the prompt recovery slows down and the slower recovery speeds up.

The challenge is to interpret these results.

Our results indicate that porous silicon is not a direct-gap semiconductor. In direct-gap semiconductors, bleaching is observed after femtosecond excitation.[45,46,52] This bleaching results from the partial occupation of the final and initial states by the photoinjected electrons and holes respectively, which decreases the absorption at all probe wavelengths and especially near the pump wavelength immediately after excitation. In the present experiments, we instead observe photoinduced absorption, which occurs either in indirect-gap semiconductors[53,54] or in amorphous semiconductors,[48,55] and is indicative

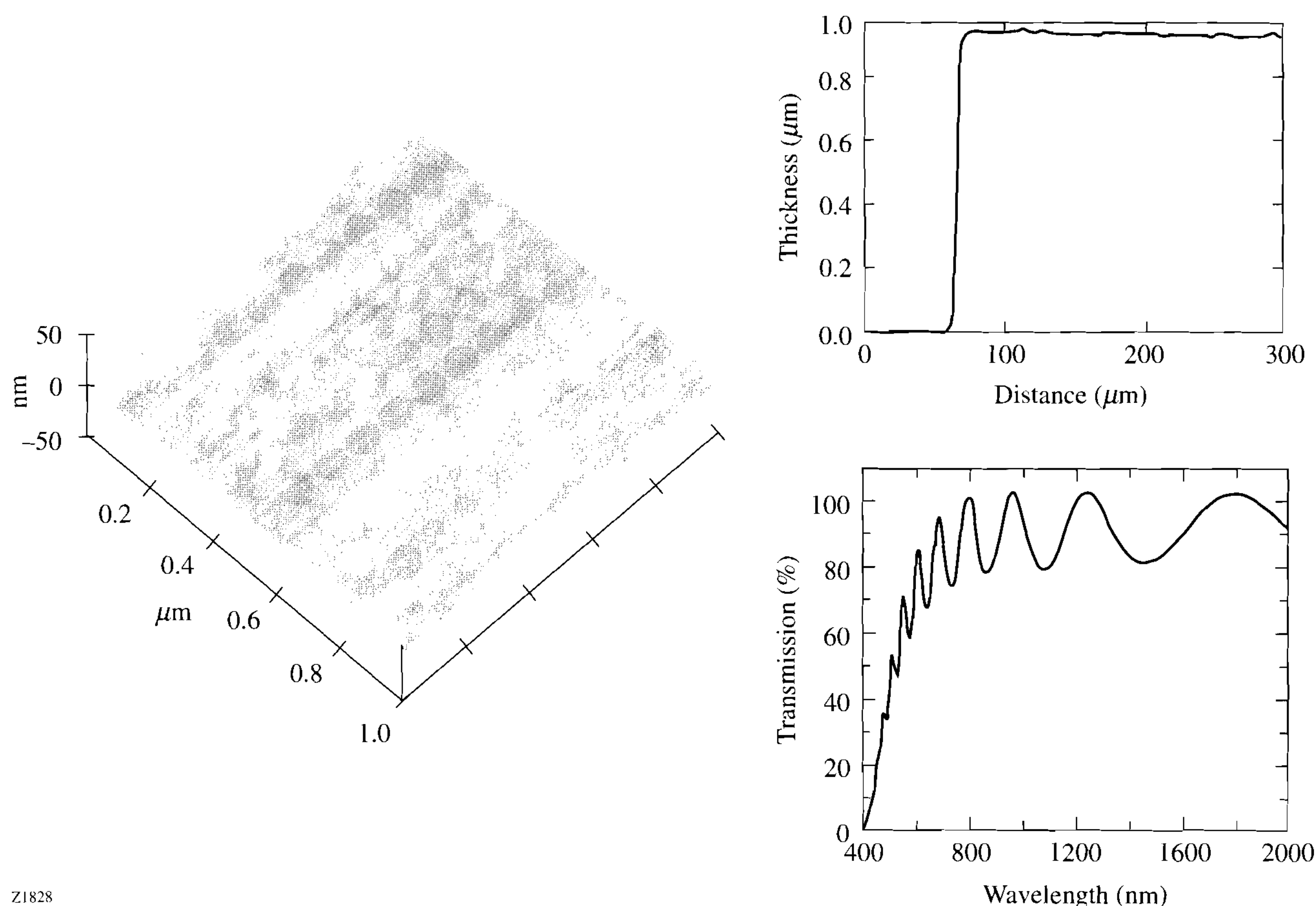

Figure 62.42
Atomic-force-micrograph, thickness measurement, and optical transmission spectrum of a thin, porous film that has been lifted off the c-Si substrate and deposited on a sapphire substrate.

of Drude absorption by free carriers. This observation confirms recent theoretical[56] and experimental[26,27] work, which also suggested that red-emitting porous silicon remains an indirect bandgap semiconductor. Figure 62.44 compares femtosecond time-resolved data obtained under similar conditions with GaAs (a direct-gap semiconductor), a-Si:H (an amorphous semiconductor), c-Si (an indirect-gap semiconductor), and porous silicon. Clearly, porous silicon and c-Si have a very similar response, which in turn is quite distinct from that of GaAs and a-Si:H.

The dynamics of the photoinduced absorption recovery are consistent with the following model. The prompt recovery is due to carrier trapping, presumably at the nanocrystallite surfaces. The fact that trapping occurs on a ~100-fs time scale should not be surprising since a classical electron moving at the thermal velocity will "hit" the surface every 30 fs. However, not all nanocrystals have a "fast" trap, and the ratio of the amplitude of the slower recovery to that of the prompt recovery is a measure of the ratio of the number of nanocrystals without a fast trap to that of nanocrystals with a fast trap. In those nanocrystals that have no fast trap, the photoinjected carriers can only recombine or be trapped in "slow" traps. Assuming that the slower recovery is due to recombination, we can explain the intensity dependence. When the number of electron-hole pairs injected per nanocrystallite is less than 1, recombination is probably radiative and relatively slow; when the number of pairs injected exceeds 1 per nanocrystal, Auger recombination becomes possible. In this process, one electron recombines with one hole, and the excess energy is given to another electron (or hole). This process is relatively efficient at large carrier densities in bulk crystalline silicon and is expected to be very efficient in nanometer-size crystallites, where the overlap between the wave functions of the carriers is strong and the momentum conservation rules that limit the Auger rate in bulk silicon are somewhat relaxed. Furthermore, the

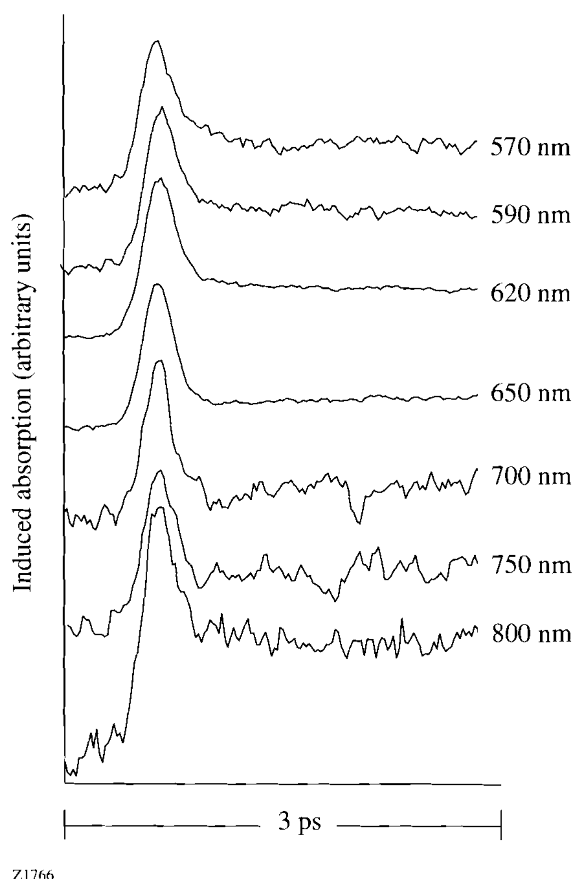

Figure 62.43
Induced absorption measured with a probe pulse at different wavelengths following carrier injection with a 100-fs-long, 2-eV pump pulse in a sample that luminesces near 1.65 eV. The traces are similar at all wavelengths.

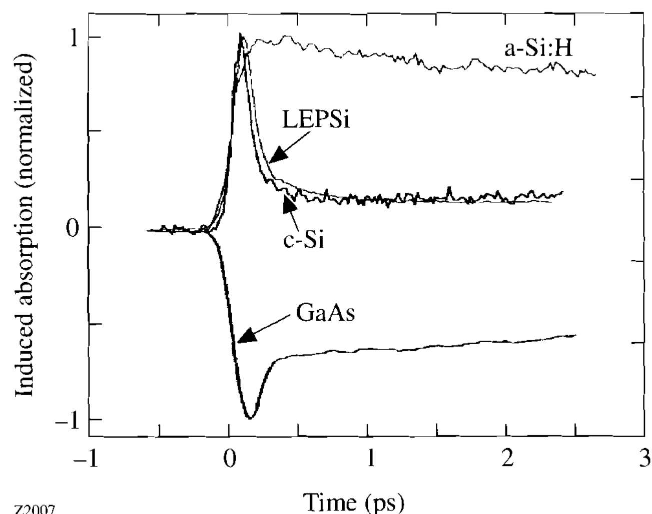

Figure 62.44
Room-temperature photoinduced absorption measurements performed in the pump-probe geometry at 2 eV in GaAs, crystalline silicon (c-Si), porous silicon (LEPSi), and amorphous hydrogenated silicon (a-Si:H).

relative amplitude of the prompt recovery is expected to decrease since in nanocrystallites with one trap the second photoinjected pair can no longer undergo fast trapping.

We thus attribute the initial recovery to trapping of the photoexcited carriers from extended states into surface states. The intensity dependence of the fast recovery is consistent with trap saturation. These traps are most likely not responsible for the luminescence because trapping tends to become more efficient when the luminescence efficiency decreases after exposure to high-intensity UV light. However, the changes in the ultrafast optical response remain small even after the luminescence efficiency drops by at least one order of magnitude.

Electroluminescent Devices

Electroluminescence (EL) was observed in LEPSi shortly after the discovery of its strong photoluminescence.[57–61] It was first detected during anodic oxidation in the electrochemical cell.[61] This EL and electrolyte electroluminescence were shown to have a spectrum similar to the PL spectrum, with an efficiency larger than 0.1%. Bsiesy *et al.*[62] reported on tuning the electrolyte EL throughout the broad PL spectrum by simply changing the applied voltage from 0.8 V to 1.5 V.[62] Cathodoluminescence has also been reported.[63,64] In this section, we focus on *solid-state* electroluminescent devices. In these light-emitting devices (LED's), electrons and/or holes are injected into the porous layer where radiative recombination occurs.

The first LED made of porous silicon was demonstrated in 1991.[57] It consisted of a metal/porous silicon/crystalline silicon structure similar to a Schottky barrier or more accurately to a metal/ insulator/semiconductor (MIS) structure. Although the device did electroluminesce, its efficiency measured at room temperature was of the order of $10^{-4}\%$ to $10^{-5}\%$. The threshold voltage for observable EL was at first very high (>> 10 V) but has since been reduced to less than 5 V. In our recent work, we have been able to detect EL for applied voltages below 1 eV in more complicated structures.[65] Such LEPSi MIS devices are very easy to fabricate since after fabrication of the porous layer, the only additional step is the evaporation of a thin metal film. Variations on this device structure have since been published by many groups. The PL and EL spectra are usually similar to each other, although in some cases not identical[66,67] for reasons that are not clear. The efficiency of these devices has remained low, although efficiencies in the range of $10^{-2}\%$ and even higher have been

quoted.[68,69] Some of the most obvious reasons for the poor efficiency are (1) the mechanism of carrier injection is not clear and possibly inefficient; (2) the semitransparent metal contacts absorb part of the luminescence; and (3) it is extremely difficult to make a good contact over the large microscopic surface area of porous silicon using line-of-sight deposition techniques. In other LED's indium tin oxide (ITO) is used as the top electrode[58] instead of a metal. This approach has several advantages, including potentially better contacts and less light absorption by the ITO. We have found in our devices that the efficiency of LED's using ITO is consistently higher than that of LED's using metals such as Au or Ag. Contacts made of conducting polymers have also been demonstrated[70] but the efficiency remained low.

The best published efficiency for porous silicon LED's was achieved using a somewhat more complicated device structure.[69] Figure 62.45 shows the proposed band structure and the current-voltage (I-V) relationship for a similar device.[66,71] The porous silicon *p-n* junction LED's were fabricated in *p*-type substrates with a resistivity of 5 to 10 Ω cm. A high-dose phosphorus implant was followed by a period of thermal annealing to yield junction depths ≤1 μm. Because holes are required in the anodization process, light assistance is essential to create *n*-type LEPSi. The LEPSi layers were thus formed by electrochemical etching in a 1:1:2 solution of HF, H_2O, and ethanol, using a constant current density of 15 mA/cm^2 for 5 to 30 min. This anodization process produces LEPSi at a rate of approximately 1 μm/min. To improve the homogeneity of the LEPSi layer, the backside of the wafers was heavily doped with boron, and a sintered Al film was used to create an intimate backside ohmic contact. Following LEPSi layer formation, a semitransparent, 100-Å gold film was deposited to form patterned 0.2-cm^2 contacts. Using similar structures, electroluminescence has been achieved from the near infrared to the blue with nearly constant efficiencies (e.g., 0.005% in the blue using indium contacts[72]).

The band diagram proposed in Fig. 62.45 is based on an analysis of the I-V curve, its temperature dependence, and the C-V data.[71] The Fermi level for *n*- and *p*-type LEPSi is taken to be ~0.2 eV above and below the midgap respectively. Thus, a small amount of band-bending is created within the LEPSi layer. The presence of a *p-n* junction in the LEPSi layer affects carrier transport, resulting in a rectifying I-V relationship that is nearly exponential in forward bias [i.e., $I = I_0\left(e^{eV/nkT} - 1\right)$]. The extracted ideality factor n was found to be 2.1 at applied forward bias voltages of less than 0.5 V and at room temperature. At higher voltages there is a large deviation from this behavior.[71]

Frequency modulation measurements were performed on LEPSi LED's.[66] In this experiment, a peak-to-peak ac signal of 10 V was applied to the device under a forward dc bias of 30 V. The modulated EL signal, detected and amplified with a lock-in amplifier, is shown in Fig. 62.46. The output power of an LED is related to the modulation frequency ω by

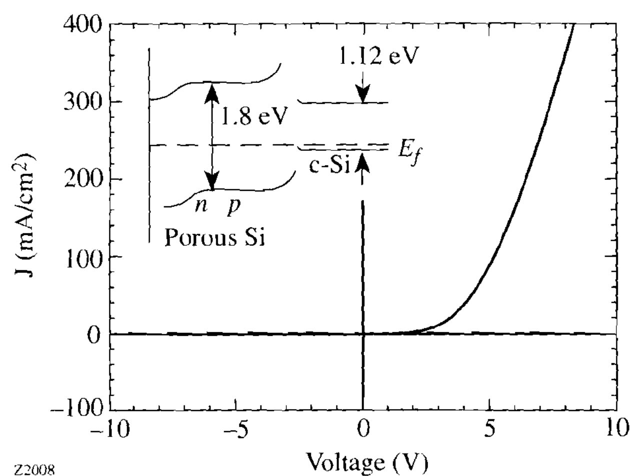

Figure 62.45
Current-voltage relationship of a light-emitting porous silicon *p-n* junction LED. The inset shows the proposed band diagram.

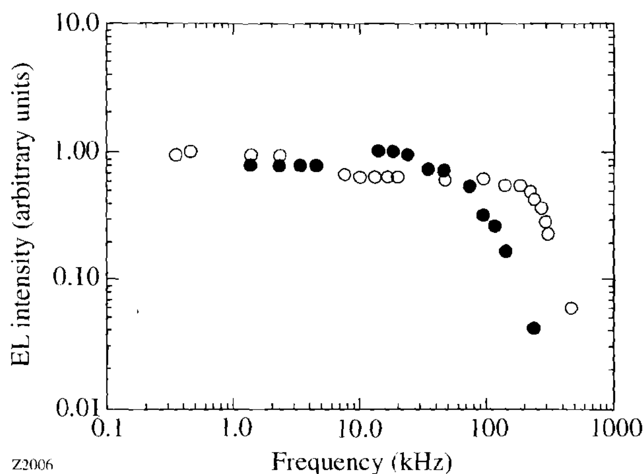

Figure 62.46
Frequency modulation response of the electroluminescence of porous silicon *p-n* junction LED's with (○) 0.2-μm junction depth and 5-μm LEPSi layer; (●) 1-μm junction depth and 10-μm LEPSi layer. The 3-dB bandwidth can exceed 100 kHz.

$$\frac{P(\omega)}{P(0)} = \left[\frac{1}{1+(\omega/\omega_0)^2}\right]^{1/2}, \quad (2)$$

where $P(0)$ is the dc power, $P(\omega)$ is the power at frequency ω, and ω_0 is the cutoff frequency. Table 62.V shows the relationship between the cutoff frequency of different device structures and the corresponding PL lifetime τ_{PL}. The fact that $2\pi/\omega_0$ is comparable to τ_{PL} suggests that the EL response is controlled by the carrier lifetime; thus, it appears that the maximum speed of the red *p-n* junction LEPSi LED's is ~1 MHz.

Table 62.V: Comparison of the EL time constant and the PL lifetime

Sample Description	$2\pi/\omega_0$ (μs)	τ_{PL} (μs)
Au/LEPSi, 30-min etching	30	13
p-n, 1 μm, 10-min etching	15	17
p-n, 0.2 μm, 5-min etching	0.86	0.7

When we prepare LEPSi MIS structures, not only is the efficiency lower but the I-V curve indicates that the transport mechanism is different and the maximum modulation speed is lower. Figure 62.47 shows that the current-voltage curve in forward bias follows a power law $I \sim V^n$, with $n > 2$ in devices where EL is detected.[67,73] Such a behavior is typical of a space-charge-limited current.[74] If the LEPSi layer can be modeled as a perfect insulator, then

$$J = \varepsilon\, \varepsilon_0\, \mu V^2/d^3,$$

where ε is the dielectric function of LEPSi, $\varepsilon_0 = 8.854\ 10^{-12}$ F/m, μ is the drift mobility in LEPSi, and d is the thickness of the LEPSi layer. If deep traps or interface traps are present, the current may increase faster than V^2, and if the mobility is electric field dependent, the current is no longer proportional to V^2. When frequency-dependent EL measurements are performed, we find as expected that the drift time across the LEPSi layer limits the device speed to at most 10 KHz.[71] Using these results, we have deduced a drift mobility of ~10^{-5} cm^2/V-s in LEPSi layers prepared from 5- to 10-Ω-cm *p*-type substrates under light assistance.[71] Finally, we note that when the LEPSi layers were prepared so that the surface passivation involved Si-O bonds and no Si-H bonds, the LED's did not degrade even after 100 h of continuous operation.[67,73]

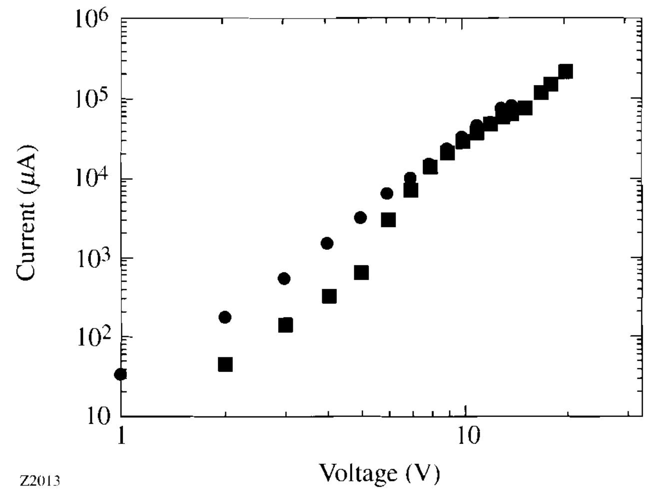

Figure 62.47
Current-voltage relationship of two metal/porous-silicon/crystalline-silicon light-emitting devices.

Prospects for Commercial Devices

Light-emitting porous silicon has given a new impetus to silicon-based optoelectronics. Since the first report of efficient photoluminescence in the red/orange part of spectrum, much progress has been achieved. Efficient luminescence has been observed from the blue/near UV to past 1.5 μm, as shown in Fig. 62.48. The quantum efficiency of LEPSi LED's has improved by at least four orders of magnitude since the first solid-state EL device was demonstrated. Nevertheless, much remains to be done before commercial applications of these materials becomes a reality.[75] Research should focus on improving either the efficiency or the speed of LED's. Better efficiencies are required for optical display applications. In addition, to be cost competitive, displays must be made using silicon thin films, and not bulk wafers. Optical interconnect applications, in contrast, do not require extremely high efficiencies but do require data-transfer rates in excess of 1 Mbit/s. Thus, for interconnects, the best hope seems to be the blue luminescence. In this section, we briefly discuss four points of relevance for technological applications. These are (1) ion implantation and oxidation of LEPSi; (2) uniformity of LEPSi; (3) mechanical stability of LEPSi; and (4) manufacture of micron-size LEPSi structures.

The major advantage of LEPSi LED's is that they could be made on the same chip as Si electronic devices or integrated circuits, which raises the important issue of their compatibility with various microelectronic processing steps. We have performed several studies[76–80] that have yielded encouraging results. Ion implantation, a technique that is widely used in

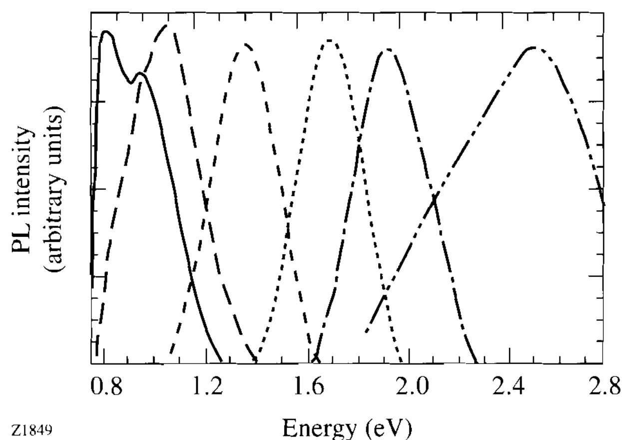

Figure 62.48
Normalized room-temperature photoluminescence spectra of various porous silicon samples, as prepared ("red" region), after oxidation ("blue" region), and after vacuum annealing ("infrared" region). The cutoff near 1.5 μm is due to the Ge photodetector.

semiconductor technology, consists of bombarding the wafer with donor or acceptor ions to produce the desired doping profile. We have demonstrated[76,77] that LEPSi can retain its strong photoluminescence after ion implantation with phosphorus and boron, provided that the dose does not exceed ~10^{14} cm^{-2}. Another important processing step is oxidation. As was discussed previously, oxidation at elevated temperatures ($T_{ox} \geq 1000°C$) produces LEPSi that emits in the blue. If the oxidation is performed at very low temperatures ($T_{ox} \leq 600°C$), the red luminescence disappears.[22,81] At these temperatures, all the hydrogen that passivated the surface of the as-grown LEPSi has been desorbed, and the oxide that is formed is of extremely poor quality. The surface is thus covered by dangling bonds,[82] which act preferentially as nonradiative recombination centers. However, as T_{ox} is raised from 600°C to ~1000°C, the quality of the thermal oxide improves, the density of dangling bonds decreases, and the PL intensity recovers. Near 1000°C, the PL intensity of high-efficiency LEPSi samples recovers to within a factor of 3 of the initial intensity. The peak PL wavelength is also blue shifted after oxidation above 600°C, in agreement with the expected decrease of the silicon crystallite size after oxidation of several silicon monolayers.[22]

For device applications, it is highly desirable that the porous layers have good cross-sectional and lateral uniformity. Previously published[83,84] studies of depth uniformity lead us to conclude that most samples are not uniform as a function of depth, with the possible exception of thin LEPSi layers prepared in the dark using p-type substrates. Spatially resolved photoluminescence and Raman measurements have shown that the first few microns usually possess a different nanostructure from that of the deeper layers. As a result, both the PL spectrum and its intensity change as a function of depth. However, we have shown[50,51] that manufacturing of LEPSi layers thicker than 10 μm with homogeneous cross-sectional PL properties is possible under specific conditions. More work must be done in this area to identify the conditions that lead to uniform LEPSi layers with good luminescence efficiency. Another issue is lateral uniformity, where we distinguish three length scales. Uniformity over large areas (>>1 cm^2) can be maintained if the electrochemical cell is designed carefully. On a scale of 1 to 100 μm, however, uniformity is more difficult to maintain. High-porosity layers tend to crack when they are removed from the solution and dried, which leads to a surface with a morphology reminiscent of a dry lake bed.[83] Spatially resolved photoluminescence (SRPL) maps of such surfaces taken with 1-μm spatial resolution show large differences in the local PL intensity, with regions that appear dark (no PL) and bright (visible PL). Even layers that show no evidence of cracking are often not homogeneous on a micron scale. Using SRPL maps, we have shown[83] that the surface of apparently uniform samples is in fact made of a very large number of small (~1-μm) regions that emit very bright PL and are separated by $\geq$1 μm. With the knowledge that longer anodization times generally produce less homogeneous surfaces, we have been able to produce LEPSi layers that appear homogeneous on a 1-μm scale by properly choosing the anodization parameters.[83] Perfect uniformity on a scale of 10 to 100 nm is almost impossible to achieve since the crystallite sizes are in the nanometer range, although the results of Fig. 62.42 show that, at least under specific conditions, the surface can be of optical quality.

As mentioned previously, high-porosity samples have a tendency to crack when dried. In addition, all LEPSi samples, with the exception of those that have been oxidized at elevated temperatures, have poor mechanical properties. A method that improves the mechanical properties and allows the production of high-porosity ($\geq$95%) films without cracking and degradation of the crystallinity has been demonstrated.[85] In this technique, the as-prepared layers are supercritically dried in CO_2 for a period of several hours. This "gentle" drying, which maintains the structural integrity of highly porous materials, has been previously used in sol-gel technology. Supercritical drying of porous silicon appears promising. Further work will help determine whether it is a necessary step for the development of LEPSi LED's.

Finally, if LEPSi LED's are to be integrated with silicon microelectronic circuits for optical interconnects or other applications, at least two developments are necessary:

- the size of the LED's must decrease from ~1 mm^2 to a few μm^2; and
- the regions of the wafer where porous silicon is not produced should be protected during anodization.

Very few studies have addressed these important issues.[78,80,86] We have developed several processes that allow us to make LEPSi lines narrower than 0.5 μm and to protect the adjacent silicon material (see Fig. 62.49). Although we have yet to demonstrate a practical device employing this feature, the ability to produce such ultranarrow lines suggests that integration of miniature porous silicon LED's with conventional VLSI is indeed possible.

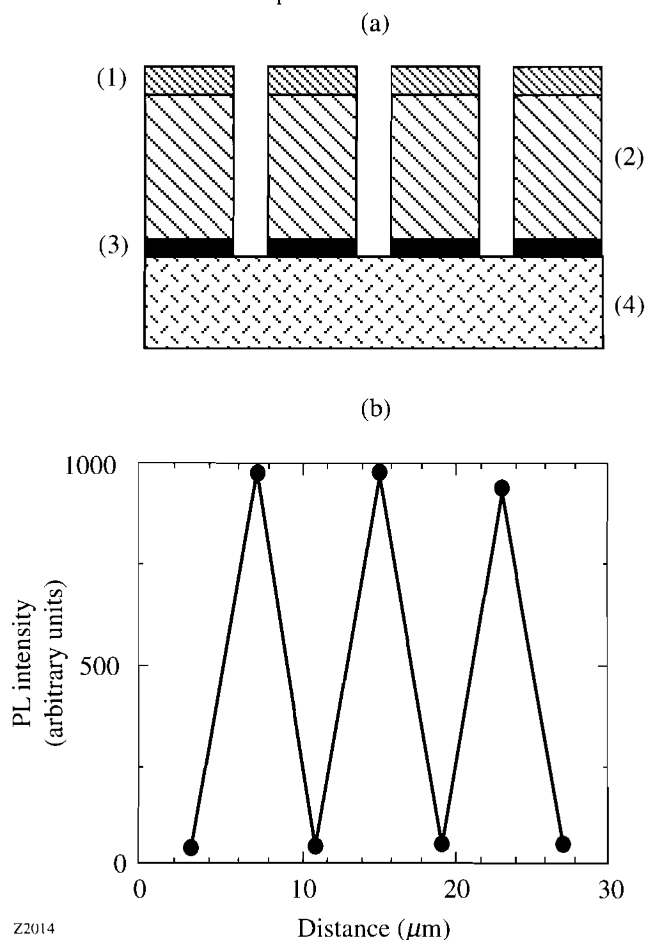

Figure 62.49
(a) Pre-anodization schematic of the mask structure. Layer (4) c-Si substrate, (3) 100-nm-thick Si_3N_4, (2) 5-μm-thick crosslinked photoresist, and (1) 1-μm-thick capping resist. (b) PL map after anodization.

Conclusions

Porous silicon, a promising new material for silicon optoelectronics, has been demonstrated to photoluminesce at room temperature with an efficiency between 0.1% and 10%. Its luminescence spectrum, intensity, and lifetime are highly sensitive to the growth and processing parameters. Light-emitting devices (LED's) made of porous silicon have already been demonstrated throughout the visible range. Since the peak of the photoluminescence spectrum of porous silicon can be changed from the blue/violet to wavelengths past 1.5 μm, it is conceivable that LED's will be made over the same range of wavelengths. Despite some impressive progress, much work still remains to be done before commercial LED's can be envisioned, even in the visible range. Nevertheless, because of its compatibility with silicon microelectronics, porous silicon is a material worthy of further scientific and technological investigations.

ACKNOWLEDGMENTS

This work was supported by grants from Rochester Gas & Electric and the New York State Energy Research & Development Authority, with additional support from the National Science Foundation Center for Photo-Induced Charge Transfer, Xerox, and Link fellowships.

REFERENCES

1. S. S. Iyer and Y.-H. Xie, Science **260**, 40 (1993).
2. J. C. Sturm *et al.*, in *Silicon-Based Optoelectronic Materials*, edited by M. A. Tischler *et al.*, Materials Research Society Symposium Proceedings, Vol. 298 (Materials Research Society, Pittsburgh, PA, 1993), pp. 69–78.
3. P. L. Bradfield, T. G. Brown, and D. G. Hall, Appl. Phys. Lett. **55**, 100 (1989).
4. F. Y. G. Ren *et al.*, in *Silicon-Based Optoelectronic Materials*, edited by M. A. Tischler *et al.*, Materials Research Society Symposium Proceedings, Vol. 298 (Materials Research Society, Pittsburgh, PA, 1993), pp. 415–423.
5. A. Uhlir, Jr., Bell Syst. Tech. J. **35**, 333 (1956).
6. G. Bomchil, A. Halimasui, and R. Herino, Microelectron. Eng. **8**, 293 (1988).
7. C. Pickering *et al.*, J. Phys. C: Solid State Phys. **17**, 6535 (1984).
8. L. T. Canham, Appl. Phys. Lett. **57**, 1046 (1990).
9. V. Lehmann and U. Gosele, Appl. Phys. Lett. **58**, 856 (1991).
10. R. L. Smith and S. D. Collins, J. Appl. Phys. **71**, R1 (1992).
11. H. Koyama and N. Koshida, J. Appl. Phys. **74**, 6365 (1993).

12. *Light Emission from Silicon*, edited by S. S. Iyer, R. T. Collins, and L. T. Canham, Materials Research Society Symposium Proceedings, Vol. 256 (Materials Research Society, Pittsburgh, PA, 1992).

13. *Microcrystalline Semiconductors: Materials Science & Devices*, edited by P. M. Fauchet *et al.*, Materials Research Society Symposium Proceedings, Vol. 283 (Materials Research Society, Pittsburgh, PA, 1993).

14. *Silicon-Based Optoelectronic Materials*, edited by M. A. Tischler *et al.*, Materials Research Society Symposium Proceedings, Vol. 298 (Materials Research Society, Pittsburgh, PA, 1993).

15. *Optical Properties of Low Dimensional Silicon Structures*, edited by D. C. Bensahel, L. T. Canham, and S. Ossicini, NATO ASI Series E, Applied Sciences, Vol. 244 (Kluwer Academic Publishers, Dordrecht, 1993).

16. *Light Emission from Silicon*, edited by J.-C. Vial, L. T. Canham, and W. Lang, (North-Holland, Amsterdam, 1994).

17. A. G. Cullis and L. T. Canham, Nature **353**, 335 (1991).

18. J. C. Vial *et al.*, in *Microcrystalline Semiconductors: Materials Science & Devices*, edited by P. M. Fauchet *et al.*, Materials Research Society Symposium Proceedings, Vol. 283 (Materials Research Society, Pittsburgh, PA, 1993), pp. 241–246.

19. Y. Kanemitsu, Phys. Rev. B **48**, 12357 (1993).

20. P. M. Fauchet, C. Peng, L. Tsybeskov, J. Vandyshev, A. Dubois, A Raisanen, T. E. Orlowski, L. J. Brillson, J. E. Fouquet, S. L. Dexheimer, J. M. Rehm, G. L. McLendon, E. Ettedgui, Y. Gao, F. Seiferth, and S. K. Kurinec, in *Semiconductor Silicon/94: Proceedings of the 7th International Symposium on Silicon Materials Science and Technology*, edited by H. R. Huff, W. Bergholz, and K. Sumino (The Electrochemical Society, Pennington, 1994), pp. 499–510.

21. L. Tsybeskov, C. Peng, S. P. Duttagupta, E. Ettedgui, Y. Gao, P. M. Fauchet, and G. E. Carver, in *Silicon-Based Optoelectronic Materials*, edited by M. A. Tischler *et al.*, Materials Research Society Symposium Proceedings, Vol. 298 (Materials Research Society, Pittsburgh, PA, 1993), pp. 307–311.

22. C. Peng, L. Tsybeskov, and P. M. Fauchet, in *Microcrystalline Semiconductors: Materials Science & Devices*, edited by P. M. Fauchet *et al.*, Materials Research Society Symposium Proceedings, Vol. 283 (Materials Research Society, Pittsburgh, PA, 1993), pp. 121–126.

23. L. Tsybeskov and P. M. Fauchet, Appl. Phys. Lett. **64**, 1983 (1994).

24. F. Koch *et al.*, in *Microcrystalline Semiconductors: Materials Science & Devices*, edited by P. M. Fauchet *et al.*, Materials Research Society Symposium Proceedings, Vol. 283 (Materials Research Society, Pittsburgh, PA, 1993), pp. 197–202; F. Koch, in *Silicon-Based Optoelectronic Materials*, edited by M. A. Tischler *et al.*, Materials Research Society Symposium Proceedings, Vol. 298 (Materials Research Society, Pittsburgh, PA, 1993), pp. 319–329.

25. *Microcrystalline and Nanocrystalline Semiconductors*, edited by R. W. Collins *et al.*, Materials Research Society Symposium Proceedings, Vol. 358 (Materials Research Society, Pittsburgh, PA, 1995).

26. P. D. J. Calcott *et al.*, J. Lumin. **57**, 257 (1993).

27. P. D. J. Calcott *et al.*, in *Microcrystalline and Nanocrystalline Semiconductors*, edited by R. W. Collins *et al.*, Materials Research Society Symposium Proceedings, Vol. 358 (Materials Research Society, Pittsburgh, PA, 1995), pp. 465–476.

28. T. van Buuren *et al.*, in *Microcrystalline and Nanocrystalline Semiconductors*, edited by R. W. Collins *et al.*, Materials Research Society Symposium Proceedings, Vol. 358 (Materials Research Society, Pittsburgh, PA, 1995), pp. 441–446.

29. S. Schuppler *et al.*, Phys. Rev. Lett. **72**, 2648 (1994).

30. M. B. Robinson *et al.*, Appl. Phys. Lett. **61**, 1414 (1992).

31. R. T. Collins, M. A. Tischler, and J. H. Stathis, Appl. Phys. Lett. **61**, 1649 (1992).

32. V. Petrova-Koch *et al.*, in *Microcrystalline Semiconductors: Materials Science & Devices*, edited by P. M. Fauchet *et al.*, Materials Research Society Symposium Proceedings, Vol. 283 (Materials Research Society, Pittsburgh, PA, 1993), pp. 179–184.

33. Y. Kanemitsu *et al.*, in *Silicon-Based Optoelectronic Materials*, edited by M. A. Tischler *et al.*, Materials Research Society Symposium Proceedings, Vol. 298 (Materials Research Society, Pittsburgh, PA, 1993), pp. 205–210.

34. L. Tsybeskov, J. V. Vandyshev, and P. M. Fauchet, Phys. Rev. B **49**, 7821 (1994).

35. J. H. Stathis and M. A. Kastner, Phys. Rev. B **35**, 2972 (1987).

36. A. Anedda *et al.*, J. Appl. Phys. **74**, 6993 (1993).

37. J. M. Rehm, G. L. McLendon, L. Tsybeskov, and P. M. Fauchet, to appear in Applied Physics Letters.

38. H. Tamura *et al.*, Appl. Phys. Lett. **65**, 1537 (1994).

39. R. E. Hummel, P. M. Fauchet, M. H. Ludwig, Ju. V. Vandyshev, S.-S. Chang, and L. Tsybeskov, to appear in Solid State Communications.

40. C. H. Perry *et al.*, in *Light Emission from Silicon*, edited by S. S. Iyer, R. T. Collins, and L. T. Canham, Materials Research Society Symposium Proceedings, Vol. 256 (Materials Research Society, Pittsburgh, PA, 1992), pp. 153–158.

41. P. M. Fauchet, E. Ettedgui, A. Raisanen, L. J. Brillson, F. Seiferth, S. K. Kurinec, Y. Gao, C. Peng, and L. Tsybeskov, in *Silicon-Based Optoelectronic Materials*, edited by M. A. Tischler *et al.*, Materials Research Society Symposium Proceedings, Vol. 298 (Materials Research Society, Pittsburgh, PA, 1993), pp. 271–276.

42. G. Mauckner *et al.*, in *Microcrystalline and Nanocrystalline Semiconductors*, edited by R. W. Collins *et al.*, Materials Research Society Symposium Proceedings, Vol. 358 (Materials Research Society, Pittsburgh, PA, 1995), pp. 489–494.

43. P. M. Fauchet, C. Peng, L. Tsybeskov, Ju. V. Vandyshev, A. Dubois, L. McLoud, S. P. Duttagupta, J. M. Rehm, G. L. McLendon, E. Ettedgui, Y. Gao, F. Seiferth, S. K. Kurinec, A. Raisanen, T. E. Orlowski, L. J. Brillson, and G. E. Carver, in *Advanced Photonics Materials for Information Technology*, edited by S. Etemad (SPIE, Bellingham, WA, 1994), Vol. 2144, pp. 34–50.

44. M. Lannoo, presented at the International School on Luminescence of Porous Silicon and Silicon Nanostructures, Les Houches, France, February 1994; M. Lannoo, C. Delerue, and G. Allan, J. Lumin. **57**, 243 (1993).

45. T. Gong, W. L. Nighan, Jr., and P. M. Fauchet, Appl. Phys. Lett. **57**, 2713 (1990).

46. J. F. Young, T. Gong, P. M. Fauchet, and P. J. Kelly, Phys. Rev. B **50**, 2208 (1994).

47. P. M. Fauchet, A. Antonetti, D. Hulin, J. Kolodzey, A. Migus, and S. Wagner, Phys. Rev. Lett. **57**, 2438 (1986).

48. P. M. Fauchet, D. Hulin, R. Vanderhaghen, A. Mourchid, and W. L. Nighan, Jr., J. Non-Cryst. Solids **141**, 76 (1992).

49. P. M. Fauchet, Y. Kostoulas, Ju. V. Vandyshev, and V. Petrova-Koch, in *Ultrafast Phenomena IX*, edited by P. F. Barbara *et al.* (Springer-Verlag, Berlin, 1994), p. 283.

50. J. von Behren, K. B. Ucer, L. Tsybeskov, Ju. V. Vandyshev, and P. M. Fauchet, to appear in the Journal of Vacuum Science and Technology (1995).

51. J. von Behren, L. Tsybeskov, and P. M. Fauchet, Appl. Phys. Lett. **66**, 1662 (1995).

52. J. L. Oudar *et al.*, Phys. Rev. Lett. **55**, 2074 (1985).

53. M. C. Downer and C. V. Shank, Phys. Rev. Lett. **56**, 761 (1986).

54. P. M. Fauchet and W. L. Nighan, Jr., Appl. Phys. Lett. **48**, 721 (1986).

55. A. Mourchid, D. Hulin, R. Vanderhaghen, W. L. Nighan, Jr., K. Gzara, and P. M. Fauchet, Solid State Commun. **74**, 1197 (1990).

56. M. S. Hybertsen, Phys. Rev. Lett. **72**, 1514 (1994).

57. A. Richter *et al.*, IEEE Electron Device Lett. **12**, 691 (1991).

58. N. M. Kalkhoran, F. Namavar, and H. P. Maruska, in *Light Emission from Silicon*, edited by S. S. Iyer, R. T. Collins, and L. T. Canham, Materials Research Society Symposium Proceedings, Vol. 256 (Materials Research Society, Pittsburgh, PA, 1992), pp. 89–94.

59. E. Bassous *et al.*, in *Light Emission from Silicon*, edited by S. S. Iyer, R. T. Collins, and L. T. Canham, Materials Research Society Symposium Proceedings, Vol. 256 (Materials Research Society, Pittsburgh, PA, 1992), pp. 23–26.

60. N. Koshida and H. Koyama, in *Light Emission from Silicon*, edited by S. S. Iyer, R. T. Collins, and L. T. Canham, Materials Research Society Symposium Proceedings, Vol. 256 (Materials Research Society, Pittsburgh, PA, 1992), pp. 219–222.

61. A. Halimaoui *et al.*, Appl. Phys. Lett. **59**, 304 (1991).

62. A. Bsiesy *et al.*, Phys. Rev. Lett. **71**, 637 (1993).

63. A. G. Cullis *et al.*, in *Microcrystalline Semiconductors: Materials Science & Devices*, edited by P. M. Fauchet *et al.*, Materials Research Society Symposium Proceedings, Vol. 283 (Materials Research Society, Pittsburgh, PA, 1993), pp. 257–262.

64. S. M. Pillai *et al.*, Jpn. J. Appl. 2, Lett. **31**, L1702 (1992).

65. L. Tsybeskov *et al.*, unpublished data.

66. C. Peng, P. M. Fauchet, K. D. Hirschman, and S. K. Kurinec, in *Microcrystalline and Nanocrystalline Semiconductors*, edited by R. W. Collins *et al.*, Materials Research Society Symposium Proceedings, Vol. 358 (Materials Research Society, Pittsburgh, PA, 1995), pp. 689–694.

67. L. Tsybeskov, S. P. Duttagupta, and P. M. Fauchet, to appear in Solid State Communications.

68. N. Koshida, presented at the International School on Luminescence of Porous Silicon and Silicon Nanostructures, Les Houches, France, February 1994.

69. P. Steiner *et al.*, in *Microcrystalline Semiconductors: Materials Science & Devices*, edited by P. M. Fauchet *et al.*, Materials Research Society Symposium Proceedings, Vol. 283 (Materials Research Society, Pittsburgh, PA, 1993), pp. 343–351; W. Lang, P. Steiner, and F. Kozlowski, J. Lumin. **57**, 341 (1993).

70. N. Koshida *et al.*, Appl. Phys. Lett. **63**, 2655 (1993).

71. C. Peng *et al.*, submitted for publication to Applied Physics Letters.

72. W. Lang, presented at the International School on Luminescence of Porous Silicon and Silicon Nanostructures, Les Houches, France, February 1994.

73. L. Tsybeskov, S. P. Duttagupta, and P. M. Fauchet, in *Microcrystalline and Nanocrystalline Semiconductors*, edited by R. W. Collins *et al.*, Materials Research Society Symposium Proceedings, Vol. 358 (Materials Research Society, Pittsburgh, PA, 1995), pp. 683–688.

74. M. A. Lampert and P. Mark, *Current Injection in Solids* (Academic Press, New York, 1970), p. 351.

75. P. M. Fauchet, in *Porous Silicon*, edited by Z. C. Feng and R. Tsu (World Scientific, Singapore, 1994), pp. 429–465.

76. C. Peng, P. M. Fauchet, J. M. Rehm, G. L. McLendon, F. Seiferth, and S. K. Kurinec, Appl. Phys. Lett. **64**, 1259 (1994).

77. C. Peng, L. Tsybeskov, P. M. Fauchet, F. Seiferth, S. K. Kurinec, J. M. Rehm, and G. L. McLendon, in *Silicon-Based Optoelectronic Materials*, edited by M. A. Tischler *et al.*, Materials Research Society Symposium Proceedings, Vol. 298 (Materials Research Society, Pittsburgh, PA, 1993), pp. 179–184.

78. S. P. Duttagupta, C. Peng, P. M. Fauchet, S. K. Kurinec, and T. N. Blanton, to appear in the Journal of Vacuum Science and Technology (1995).

79. S. P. Duttagupta, L. Tsybeskov, P. M. Fauchet, E. Ettedgui, and Y. Gao, in *Microcrystalline and Nanocrystalline Semiconductors*, edited by R. W. Collins *et al.*, Materials Research Society Symposium Proceedings, Vol. 358 (Materials Research Society, Pittsburgh, PA, 1995), pp. 381–386.

80. S. P. Duttagupta, P. M. Fauchet, C. Peng, S. K. Kurinec, K. Hirschman, and T. N. Blanton, in *Microcrystalline and Nanocrystalline Semiconductors*, edited by R. W. Collins *et al.*, Materials Research Society

Symposium Proceedings, Vol. 358 (Materials Research Society, Pittsburgh, PA, 1995), pp. 647–652.

81. V. Petrova-Koch *et al.*, Appl. Phys. Lett. **61**, 943 (1992).

82. H. Linke *et al.*, in *Microcrystalline Semiconductors: Materials Science & Devices*, edited by P. M. Fauchet *et al.*, Materials Research Society Symposium Proceedings, Vol. 283 (Materials Research Society, Pittsburgh, PA, 1993), pp. 251–256.

83. E. Ettedgui, C. Peng, L. Tsybeskov, Y. Gao, P. M. Fauchet, G. E. Carver, and H. A. Mizes, in *Microcrystalline Semiconductors: Materials Science & Devices*, edited by P. M. Fauchet *et al.*, Materials Research Society Symposium Proceedings, Vol. 283 (Materials Research Society, Pittsburgh, PA, 1993), pp. 173–178.

84. F. Kozlowski and W. Lang, J. Appl. Phys. **72**, 5401 (1992).

85. L. T. Canham *et al.*, Nature **368**, 133 (1994).

86. N. M. Kalkhoran, in *Microcrystalline Semiconductors: Materials Science & Devices*, edited by P. M. Fauchet *et al.*, Materials Research Society Symposium Proceedings, Vol. 283 (Materials Research Society, Pittsburgh, PA, 1993), pp. 365–370.